applied sciences

MDPI

Article

A Numerical Study on the Cement Slurry Penetration Performance of the Cyclic Grouting Method with High-Frequency Pulsating Pressure

Yongfeng Li [1,2], Xiaobin Chen [3], Jianzhong Li [1], Lubo Tang [3,*], Fantong Lin [4] and Xinxin Zhang [1]

[1] School of Geosciences and Info-Physics, Central South University, Changsha 410083, China; lijianzhong@csu.edu.cn (J.L.)
[2] Powder China Zhongnan Engineering Co., Ltd., Changsha 410014, China
[3] School of Civil Engineering, Central South University, Changsha 410083, China
[4] Institute of Defense Engineering, AMS, PLA, Beijing 100850, China
* Correspondence: tanglubo@csu.edu.cn

Abstract: The performance of traditional steady grouting is sometimes limited; therefore, a new high-frequency pulsed grouting method is proposed. Through the CFD method, this paper studies the cement slurry penetration performance of cyclic grouting under the influence of pulsating pressure and steady pressure. Firstly, the penetration shape and flow fields of the two grouting methods are investigated. Secondly, the effects of pulsation parameters on penetration performance are studied. Finally, the influence of various working conditions, such as soil properties, grout parameters, grouting pipe length, and back pressure, on penetration distance is also investigated. The results show that pulsating grouting achieves better penetration performance compared with steady pressure grouting. With the increase in frequency, pulsating grouting exhibits superior performance, while with the increase in pulsation amplitude, the penetration distance initially increases and then decreases. This is because part of the pulsating pressure is lower than the back pressure, which weakens the pulsating effect. As viscosity and back pressure increase and as porosity and particle size decrease, the proportion of lateral diffusion in pulsating grouting relative to steady pressure grouting increases. This indicates that lateral penetration performance achieves optimal results under high-flow-resistance conditions. However, when the flow resistance becomes excessively high, the vertical penetration distance may be affected. This study is expected to improve the grouting efficiency and provide a better understanding of pulsating grouting design and operation.

Keywords: cement slurry; penetration behavior; pulsating pressure; high-frequency grouting

check for updates

Citation: Li, Y.; Chen, X.; Li, J.; Tang, L.; Lin, F.; Zhang, X. A Numerical Study on the Cement Slurry Penetration Performance of the Cyclic Grouting Method with High-Frequency Pulsating Pressure. *Appl. Sci.* **2023**, *13*, 11919. https://doi.org/10.3390/app132111919

Academic Editor: Laurent Daudeville

Received: 13 October 2023
Revised: 27 October 2023
Accepted: 29 October 2023
Published: 31 October 2023

Copyright: © 2023 by the authors. Licensee MDPI, Basel, Switzerland. This article is an open access article distributed under the terms and conditions of the Creative Commons Attribution (CC BY) license (https://creativecommons.org/licenses/by/4.0/).

1. Introduction

Grouting technology refers to the process of injecting slurry into soil layers to improve the strength and or prevent seepage [1]. The technology is widely utilized in areas such as tunnel construction, underground pipeline repair, mining engineering, and oil fields. This technology has attracted extensive attention, and various grouting methods have been gradually proposed. Among these methods, cyclic grouting is widely used in underground engineering, especially in soft soil layers, due to its ability to prevent the accumulation of grout and its cost-effectiveness [2]. During the grouting process, steady pressure is typically employed [3]. However, with the increasing complexity of construction projects, steady pressure grouting may not meet the requirements under some working conditions [4]. For example, the water gushing in tunnels, subsidence of underground structures, and debris flow in slopes can create uneven pore channels in the soil. Under steady pressure, the slurry will penetrate along the dominant channels and slurry particles are prone to block the small pore channels [5]. This results in low grouting efficiency and significant economic losses.

In recent years, pulsating grouting has been proposed and has attracted extensive attention. This pulsating method is mainly achieved through intermittent pressure provided with the pressure pump. Zhao [6] presented that pulsating pressure can alleviate particle blockage phenomena, which is beneficial for slurry penetration. Ghafar [7] found that pulsating pressure can induce a transition between laminar and turbulent flow fields, reducing flow resistance and alleviating slurry filtration. Dou [5] presented that pulsating pressure can weaken the guiding effect of dominant channels, making the grout penetration more controllable. Zhang [8] investigated the mechanical behavior of pulsating grouting, and it was found that the strength of the stone body grouted using pulsating pressure is higher. Through electron microscope scans, Zhang [4] found that the soil aggregates grouted using pulsating grouting exhibit a clustered structure, which is denser compared to the flocculent structure observed after steady pressure grouting.

However, due to the absence of pressure during pulsation intervals, researchers found that intermittent pressure grouting may sometimes reduce the slurry flow rate and weaken the advantage of the pulsation effect [9]. Hence, research on the effect of pulsating frequency on grouting performance is conducted. Wakita [10] found that high-frequency oscillations can reduce the viscosity of the slurry, thereby increasing the penetration distance within rock fractures. Mohammed [11] used a 'Haskel' pump to generate continuous pressure pulsations (3 Hz) and found that this dynamic pressure significantly enhanced the grouting efficiency. Research conducted by Ghafar [7] and Dou [5] also suggests that the higher frequency is more advantageous for the penetration of the slurry. However, the effects of pulsation parameters, soil parameters, and various working parameters on the slurry require further research.

Hence, in order to promote the application of efficient grouting technology in soil layers, this study compared the penetration performance of high-frequency pulsating grouting with steady pressure grouting. Subsequently, this paper studied the mechanism for the superior performance of pulsating grouting. Finally, the effect of pulsating frequency, pressure pulse amplitude, soil parameters, slurry parameters, back pressure, and length of grouting pipes on penetration distance is investigated. This study can provide new perspectives for investigating the slurry penetration performance under different pulsating parameters.

2. Methodology

2.1. Grouting Method and Slurry Material

The schematic diagram of cyclic grouting is shown in Figure 1. Under medium-to-high pressure, the grout within the annular space is injected into the soil, and the portion of grout that is not absorbed by the soil will be returned to the grout storage tank. This method creates a circulation of slurry flow within the grouted borehole, preventing the clogging of slurry particles. In order to mitigate the size effect, the grouting area is chosen to be 20 m × 20 m [2]. The diameter of the borehole is 96 mm. The currently commonly used grouting method is the first type, steady pressure. Recently, there has been an emergence of an intermittent pressure method to introduce pulsations. However, this method is difficult to control and has low flow rates. Therefore, this paper proposes the adoption of a high-frequency pulsating pressure grouting method.

Cement slurry is a common particle grouting material with high strength, low cost, and wide applicability [12,13]. Due to the long length of the grouting pipe during cyclic grouting, cement slurry typically employs a high water-to-cement ratio to ensure a certain level of fluidity. When the water–cement ratio is high, cement slurry can be considered as Newtonian fluid. Therefore, the rheological model of cement slurry in this paper adopts the Newtonian fluid model. And the soil splitting has been overlooked; the grouting mechanism was simplified as penetration grouting. The expression of the Newtonian fluid model is given in Equation (1) [1].

$$\tau = \mu \cdot \gamma \tag{1}$$

where τ is the shear stress, μ is the dynamic viscosity, γ is the shear rate.

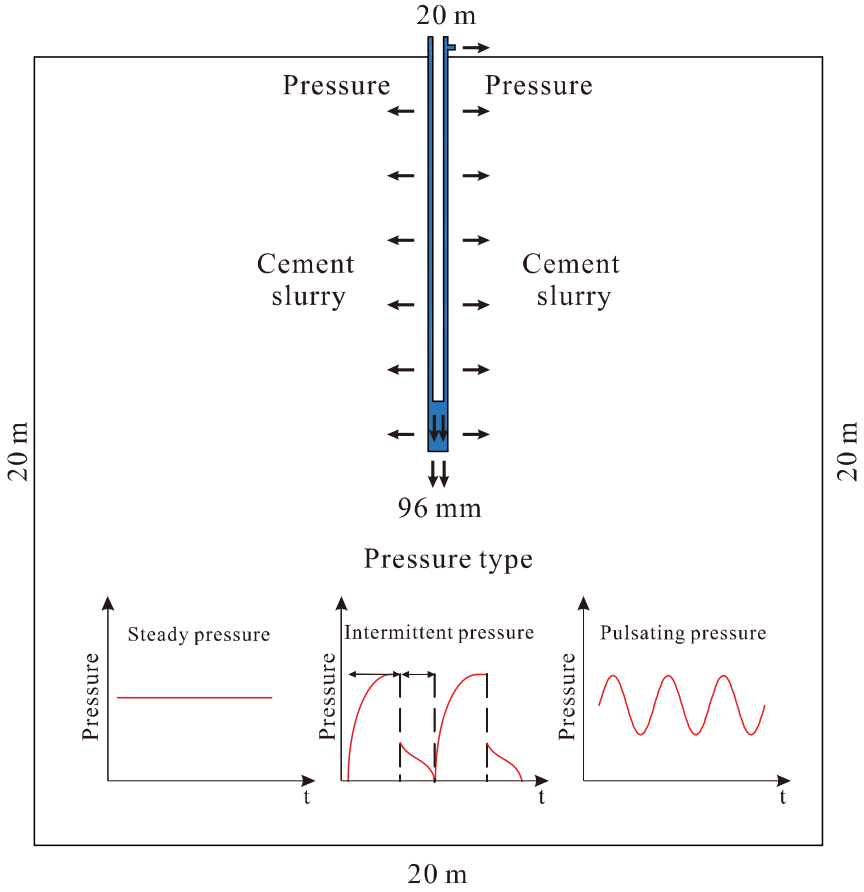


Figure 1. Schematic of the numerical model and pressure type.

2.2. Methodology of Numerical Simulation

The Computational Fluid Dynamics (CFD) method is a commonly used method in grouting processes. CFD can simulate a wide range of complex fluid phenomena, including multiphase flows and turbulence [14,15]. CFD can also provide more detailed information compared to experiments, offering insights into parameters like velocity and pressure distributions [16]. These details are crucial for a deeper understanding of fluid behavior and performance optimization. Hence, the CFD method is adopted in this paper.

2.3. Multiphase Flow Model and Turbulent Model

The Volume of Fluid (VOF) method is a widely used multiphase flow method. This method provides a sharp representation of fluid interfaces, which is particularly valuable for capturing details involving complex flows. The specific governing equations are as follows [17]:

The mass conservation equation is

$$\frac{\partial \rho}{\partial t} + \nabla \cdot (\rho \overline{U}) = 0 \tag{2}$$

The momentum equation can be expressed as

$$\frac{\partial (\rho \overline{U})}{\partial t} + \nabla \cdot \left(\rho \overline{U} \overline{U}\right) = -\nabla P + \nabla \left[\mu \left(\nabla \overline{U} + \nabla \overline{U}^T\right)\right] + \rho \overline{g} \tag{3}$$

where ρ is the density of the fluid, $\overline{U}$ is the velocity vector of the fluid, μ represents the kinematic viscosity coefficient, P represents pressure, and $\overline{g}$ is the gravitational acceleration.

The VOF method exploits a phase fraction F_P to represent the volume fraction. It ranges from zero to one, where $F_P = 0$ represents air, $F_P = 1$ represents slurry, and $0 < F_P < 1$

represents a two-phase interface. The phase transformation equation and the properties of the fluid can be written as

$$\frac{\partial F_P}{\partial t} + \mathbf{U} \cdot \nabla F_P = 0 \tag{4}$$

$$\rho = (1 - F_\mathrm{P})\rho_\mathrm{A} + F_\mathrm{P}\rho_\mathrm{P} \text{ and } \mu = (1 - F_\mathrm{P})\mu_\mathrm{A} + F_\mathrm{P}\mu_\mathrm{P} \tag{5}$$

Due to the fluctuating pressure, turbulent behavior occurs within the computational domain.

The realizable k-ε model enhances the physical realism of the turbulence predictions by incorporating more accurate terms and coefficients [18]. It also takes into account the anisotropic nature of turbulence, which is especially important for flows with significant directional variations. Therefore, this model is adopted in this study, and the expressions are as follows [18]:

$$\frac{\partial}{\partial t}(\rho k) + \frac{\partial}{\partial x_j}(\rho k u_j) = \frac{\partial}{\partial x_j}\left[\left(\mu + \frac{\mu_t}{\sigma_k}\right)\frac{\partial k}{\partial x_j}\right] + G_k + G_b - \rho\varepsilon - Y_M + S_k \tag{6}$$

$$\frac{\partial}{\partial t}(\rho\varepsilon) + \frac{\partial}{\partial x_j}(\rho\varepsilon u_j)\& = \frac{\partial}{\partial x_j}\left[\left(\mu + \frac{\mu_t}{\sigma_x}\right)\frac{\partial \varepsilon}{\partial x_j}\right] + \rho C_i S\varepsilon - \rho C_2 \frac{\varepsilon^2}{k + \sqrt{v\varepsilon}} + C_{1\varepsilon}\frac{\varepsilon}{k}C_{3\varepsilon}G_b + S_\varepsilon \tag{7}$$

In the equation, G_k represents the generation term of turbulent kinetic energy caused by Reynolds-averaged velocity gradients. σ_k and σ_ε are the Prandtl numbers for turbulent kinetic energy and dissipation rate, respectively. G_b represents the turbulent kinetic energy (J) generated due to buoyancy, and Y_M represents the contribution of fluctuation expansion in compressible turbulence to the overall dissipation rate. S_k and S_ε are user-defined source terms. $C_{1\varepsilon}$, $C_{2\varepsilon}$, and $C_{3\varepsilon}$ represent the numerical constants.

2.4. Solving Strategies

The Pressure Implicit with Splitting of Operators (PISO) method is a commonly used iterative algorithm for solving fluid dynamics problems. This method handles the coupling between velocity and pressure fields through an iterative process, enabling more accurate capturing of pressure and velocity variations in the flow field. Hence, the coupled velocity and pressure problem is addressed using the PISO algorithm [17].

The momentum equation at convergence can be semi-discretized as follows:

$$A_P\mathbf{U}_p^{t+\Delta t} + \sum A_N\mathbf{U}_N^{t+\Delta t} - \mathbf{S}_P^t = -\frac{1}{V_P}\sum p_f^{t+\Delta t}\mathbf{S}_f \tag{8}$$

where A_P and A_N are coefficients related to the present element P and adjacent element N, respectively, $\boldsymbol{U}_p^0$ is the volumetric velocity of element P, and $\mathbf{S}_p^t$ is the current acceleration at the center of element P, with the superscript t representing the current time step.

According to Equation (8), the volumetric velocity $\mathbf{U}_p^{t+\Delta t}$ is described as

$$\mathbf{U}_p^{t+\Delta t} = \mathbf{HbyA}_P^{t+\Delta t} - \frac{1}{A_P}\frac{1}{V_P}\sum p_f^{t+\Delta t}\mathbf{S}_f \tag{9}$$

where $\mathbf{HbyA}_P^{t+\Delta t}$ is the spatial convective and diffusive fluxes expressed with finite volume representation, and it can be written as

$$\mathbf{HbyA}_P^{t+\Delta t} = \frac{1}{A_P}\left(-\sum A_N\mathbf{U}_N^{t+\Delta t} + \mathbf{S}_P^n\right) \tag{10}$$

Similarly, the volumetric velocity at cell face f is

$$\mathbf{U}_{p,f}^{t+\Delta t} = \mathbf{HbyA}_{P,f}^{t+\Delta t} - \frac{1}{A_{P,f}}\left(\frac{1}{V_P}\sum p_f^{t+\Delta t}\mathbf{S}_f\right)_f \tag{11}$$

Based on the convergence situation, the discretized form of the continuity equation is written as

$$\sum\left(\mathbf{U}_{P,f}^{t+\Delta t}\cdot\mathbf{S}_f\right)=0 \tag{12}$$

where $\mathbf{U}_{p,f}^{t+\Delta t}$ is the volumetric velocity of element P at the cell face f when the time is $t+\Delta t$, and $\mathbf{S}_f$ is the exterior normal vector at the cell face f.

By substituting Equation (11) into Equation (12), an expression with pressure and velocity is obtained.

$$\sum\mathbf{HbyA}_f^{t+\Delta t}\cdot\mathbf{S}_f=\sum\frac{1}{A_{P,f}}\left(\frac{1}{V_P}\sum p_f^{t+\Delta t}\mathbf{S}_f\right)_f\cdot\mathbf{S}_f \tag{13}$$

The discretized form of Equation (13), which is also known as the Poisson pressure equation, can be written as

$$\nabla\cdot\mathbf{HbyA}^{t+\Delta t}=\nabla\cdot\left(\frac{1}{A}\nabla p^{t+\Delta t}\right) \tag{14}$$

By solving Equation (14), the convergent pressure can be calculated. Based on it, the new velocity and normal flux of the volumetric velocity will be updated. The solution procedure of the PISO is shown in Figure 2.

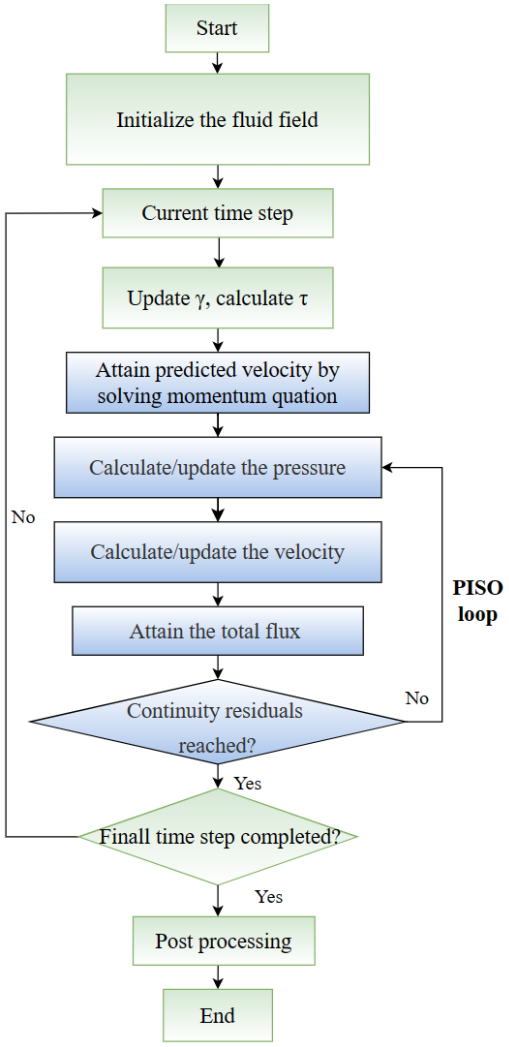


Figure 2. Solution procedure of the PISO.

The second order upwind was employed for calculating turbulent kinetic energy and turbulent dissipation rate. This method can accurately capture the change of flow field and reduce the numerical dissipation, which is thus adopted in this paper.

2.5. Boundary Conditions and Time Step

As shown in Figure 3, the computational domain is divided into two parts. One part is the annular space between the wellbore and the grouting pipe, named fluid 1. Since this part is empty, no resistance is set. The inlet is set as the pressure inlet, in which the pressure of pulsating grouting is a sinusoidal wave and the pressure of steady grouting is constant [11]. The grouting pipe is defined as the wall. The pressure outlet is set on the ground to recycle the circulating slurry. The other part is the soil, which is named as fluid 2. Fluid 2 is defined as a homogeneous porous medium, and the flow resistance is computed using the Ergun equation, expressed as follows [18]:

$$\frac{|\Delta p|}{L} = \frac{150\mu}{D_p^2}\frac{(1-\varepsilon)^2}{\varepsilon^3}v_\infty + \frac{1.75\rho}{D_p}\frac{(1-\varepsilon)}{\varepsilon^3}v_\infty^2 \tag{15}$$

where Δp represents the pressure drop, μ is the dynamic viscosity, ε is the porosity, v_∞ denotes the fluid velocity, D_p is the particle diameter, ρ stands for the fluid density, and L signifies the length of the porous region. The viscous and inertial loss coefficient in each component direction may be identified as

$$\alpha = \frac{D_p^2}{150}\frac{\varepsilon^3}{(1-\varepsilon)^2} \text{ and } C_2 = \frac{3.5}{D_p}\frac{(1-\varepsilon)}{\varepsilon^3} \tag{16}$$

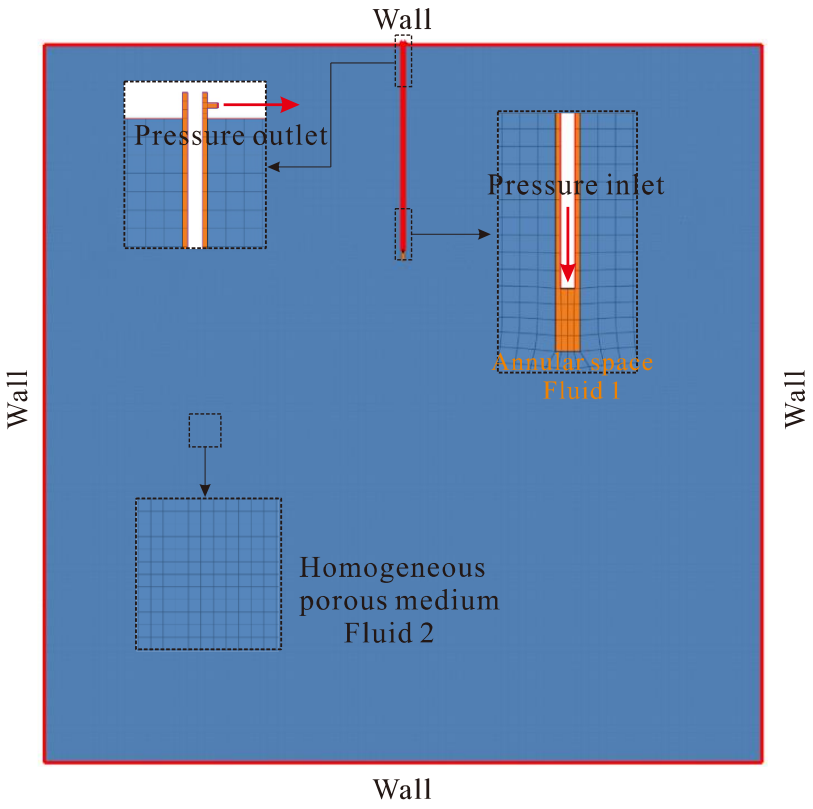


Figure 3. Boundary condition of computational domain.

Simulating pressure fluctuations accurately typically requires around 50 time steps within one sinusoidal period. Considering the effects of flow resistance and slurry properties on convergence, the time step is set to 5 e-4 s. In this study, the highest frequency

is 3.5 Hz, so there are 571 time steps within one cycle, which is sufficient to accurately describe pressure fluctuations.

3. Results and Discussion

In this section, the grouting process was introduced, and then the differences in the flow field between pulsating grouting and steady pressure grouting were studied. The effects of pulsating frequency, pressure pulse amplitude, porosity, particle size, viscosity, length of grouting pipe, and back pressure on penetration distance were also investigated.

3.1. Penetration Process of Cyclic Grouting

The penetration process of cyclic grouting is shown in Figure 4. In the initial stage, the slurry mainly flows downward (as shown in t1 moment). Due to the high flow resistance of the soil below the grout pipe, slurry begins to flow upward along the annular space (as shown in t2 moment). As shown in the t3 moment, the slurry penetrating along the left annular space is faster than that on the right side. This is because the back pressure generated with the outlet hinders the flow of slurry in the right-side annular channel. As the slurry spreads, both sides of the annular space become filled with slurry (as shown in t4 moment). Subsequently, under the influence of grouting pressure, the slurry penetrates both sides. In the middle stages of the grouting process, the penetration distance at the lower part of the grouting pipe is greater than the upper part (as shown in t5–t6 moment). As the grouting process continues, the shape of slurry penetration exhibits a typical columnar pattern (as shown in t7–t8 moment).

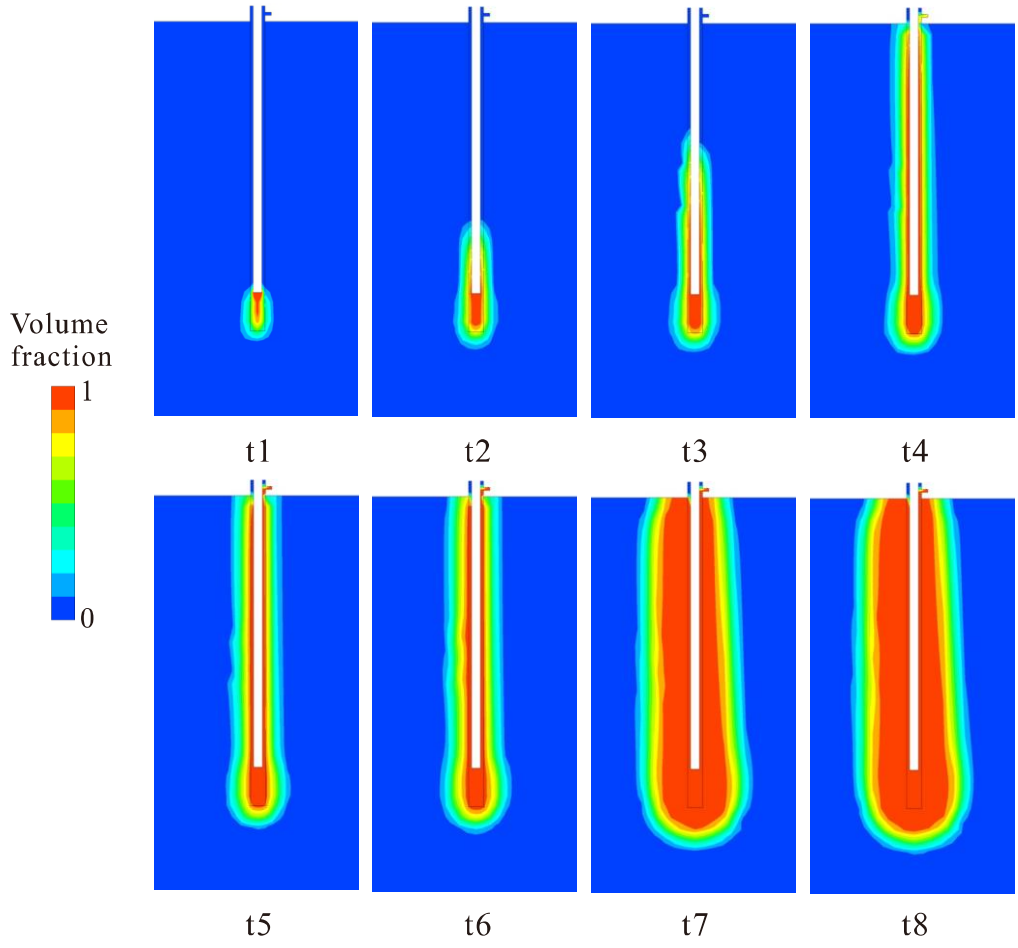


Figure 4. Penetration shape of cyclic grouting.

Because the soil in this study is assumed to be a homogeneous porous medium, the penetration shapes of pulsating grouting and steady pressure grouting are similar. However, it was observed that the penetration distance of pulsating grouting is larger than that of steady pressure grouting. In order to analyze the reasons, the streamlines of the flow field for both grouting methods were monitored. For the convenience of observation, the maximum value of streamline velocity was fixed. Therefore, a larger area with streamline velocity indicates higher velocity within the flow field, whereas a smaller area suggests lower velocity within the flow field. The streamlines of the steady pressure grouting are shown in Figure 5. Since the velocity of the streamlines in other areas of the flow field is almost zero, we only selected the streamlines in the effective region. It can be observed that as the grouting progresses, due to the increase in flow resistance, the grouting velocity under steady pressure decreases.

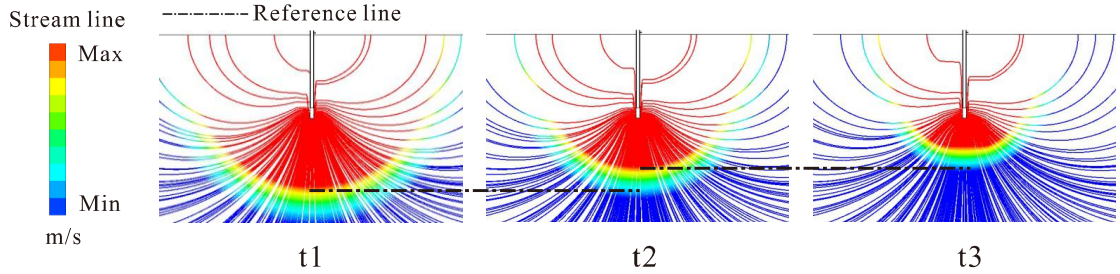


Figure 5. Steam line of steady grouting.

Figure 6 presents the steam line of the pulsating grouting method, and it can be found that the slurry velocity is periodic due to cyclic variations in pressure. At times t1 to t3, the slurry velocity gradually increases, while at times t4 to t6, the slurry velocity decreases. Subsequently, the velocity of the slurry will increase again and then experience periodic changes. When resistance within the calculation domain is high, the performance of steady pressure grouting may be limited, while this pulsation effect can improve penetration distance [7].

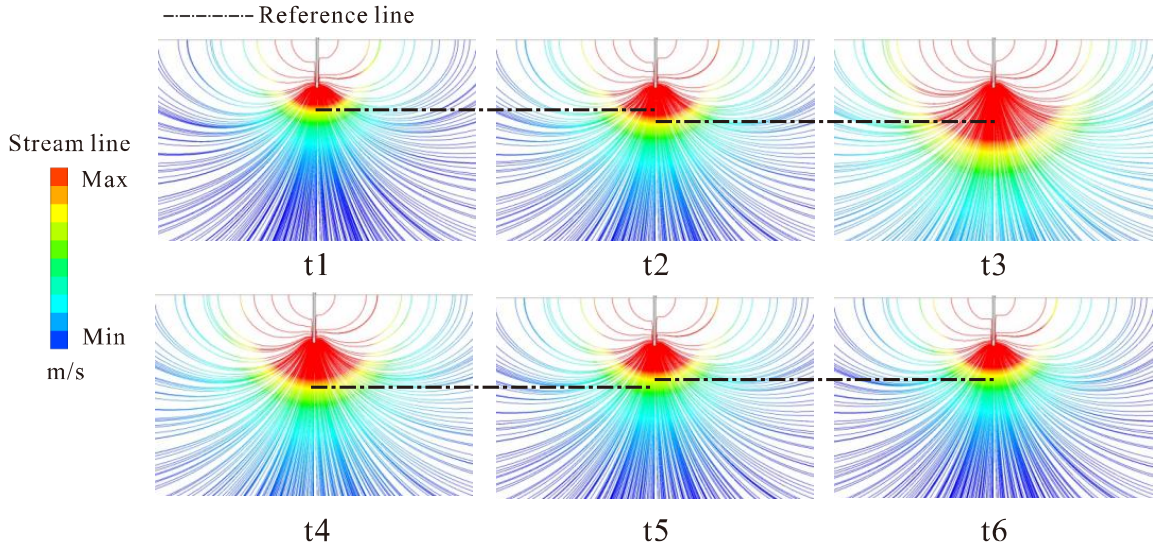


Figure 6. Steam line of pulsating grouting.

3.2. Effect of Pulsating Parameters on Penetration Distance

There are mainly two pulsation parameters: one is the pulsating frequency, and the other is the pressure pulse amplitude. When comparing the performance of the two grouting methods, the average value of the sinusoidal pressure is taken as the pressure for steady pressure grouting, and all other parameters are kept consistent.

Figure 7 illustrates the impact of pulsation frequency on the slurry diffusion for both grouting methods. The average pressure is 4 MPa, the porosity is 0.3, the average particle size is 1 mm, the viscosity of the slurry is 0.18 Pa·s, the pressure pulse amplitude is 0.5 MPa, and the back pressure is set to 2 MPa. The purple line represents the lateral penetration distance, and the orange line represents the vertical penetration distance. The solid lines represent the penetration distances for pulsating grouting at different frequencies, and the dashed line represents the penetration distance for steady pressure grouting. Since steady pressure grouting does not have a pulsating frequency, the dashed line is a straight line. It can be observed that the penetration distance of pulsating grouting is always greater than that of steady pressure grouting. And with the increase in frequency, the penetration distance of pulsating pressure grouting also increases; this phenomenon is similar to the results observed by researchers [5]. Both the lateral and vertical penetration distance follows an exponential distribution, and the expressions are $Y = \exp(5.52 + 0.138X - 0.016X^2)$ and $Y = \exp(4.94 + 0.25X - 0.037X^2)$, respectively. At a frequency of 3.5 Hz, the lateral and vertical diffusion distances increased by 70 mm and 60 mm compared to steady pressure grouting.

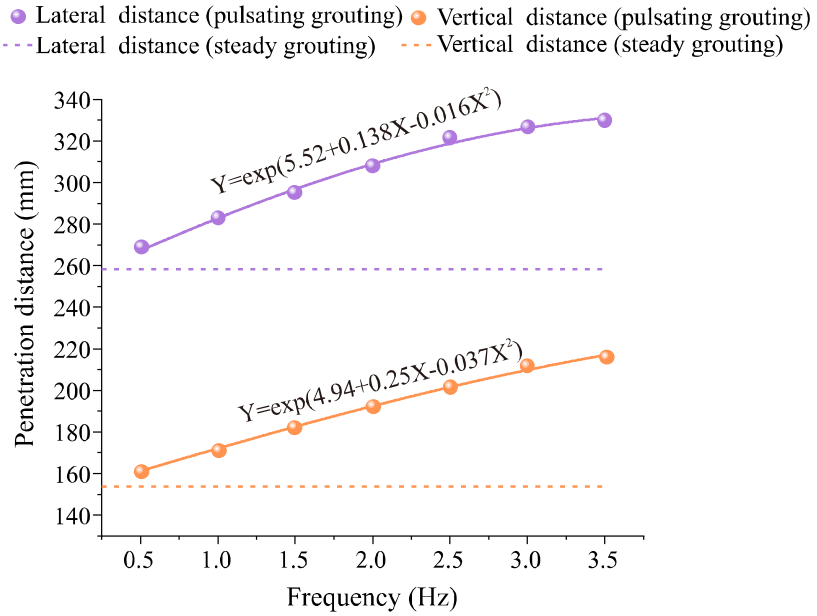


Figure 7. Effect of pulsating frequency on penetration distance.

Figure 8 shows the effect of pressure pulse amplitude on penetration distance. The average pressure is 4 MPa, the porosity is 0.3, the average particle size is 1 mm, the viscosity of the slurry is 0.18 Pa·s, the pulsating frequency is 2.5 Hz, and the back pressure is 2 MPa. It can be found that the penetration distance of pulsating grouting is still greater than that of steady pressure grouting. However, both the lateral distance and vertical distance increase initially and then decrease with the increase in pressure amplitude, with the turning point occurring at the pressure amplitude of 2 MPa. This is because the average pressure of the sinusoidal pressure is 4 MPa (which is consistent with steady pressure), and the back pressure at the outlet is 2 MPa. When the pressure amplitude exceeds 2 MPa, a part of the pressure pulsation is less than the back pressure. This means that the pressure inside the annulus will be lower than the pressure at the outlet, which hinders the upward movement of the slurry. The lateral penetration distance follows an exponential distribution, with $Y = \exp(5.6 + 0.23X - 0.057X^2)$, while the vertical penetration follows $Y = \exp(5.1 + 0.29X - 0.007X^2)$. When the pressure pulse amplitude is 2 MPa, the lateral and vertical diffusion distances increased by 72 mm and 50 mm, compared to steady pressure grouting.

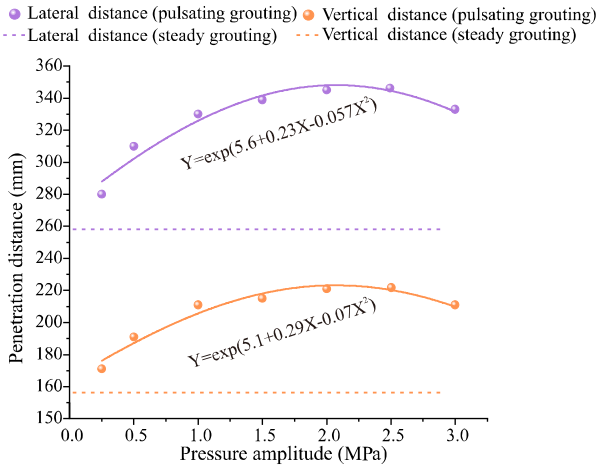


Figure 8. Effect of pressure pulse amplitude on penetration distance.

3.3. Effect of Working Conditions on Penetration Distance

In this section, the effect of various working conditions (porosity, average particle size, viscosity, grouting pipe length, and back pressure) on the penetration distance is discussed. Figures 9 and 10 show the effect of porosity on penetration distance. The percentage increase in distance is defined as

$$\frac{distance\ of\ pulsating\ grouting - distance\ of\ steady\ grouting}{distance\ of\ steady\ grouting} \quad (17)$$

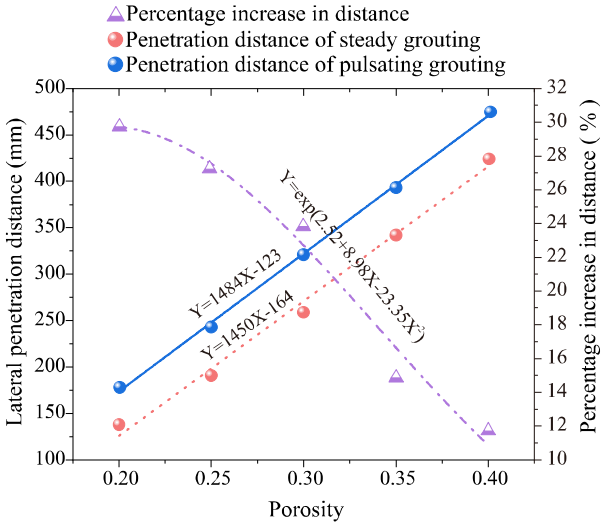


Figure 9. Effect of porosity on lateral penetration distance.

As shown in Figure 9, it can be observed that with the increase in porosity, the lateral penetration distances of both pulsating grouting and steady grouting increase linearly. The expressions are Y = 1484X − 123 and Y = 1450X − 164, respectively. However, as the porosity increases, the percentage increase in distance gradually decreases from 29.7–19.7%, following the expression Y = exp (2.52 + 8.98X − 23.35X^2). This indicates that pulsating grouting performs better under high resistance. As shown in Figure 10, the vertical penetration distance of pulsating grouting and steady grouting also increases linearly, with the expressions Y = 996X − 106.6 and Y = 932X − 115.6, respectively. However, the percentage increase in distance exhibits a trend of initially increasing and then decreasing. This is because when the porosity is low, the slurry tends to flow towards the annular area with lower flow resistance rather than into the soil below the grouting pipe. As a result, when the porosity decreases from 0.25 to 0.2, due to the faster diffusion of the slurry under

the influence of pulsation, more slurry flows into the annular space, which reduces the percentage increase in distance. With the increase in porosity, the flow resistance decreases, and the patterns for lateral and vertical penetration behavior become similar.

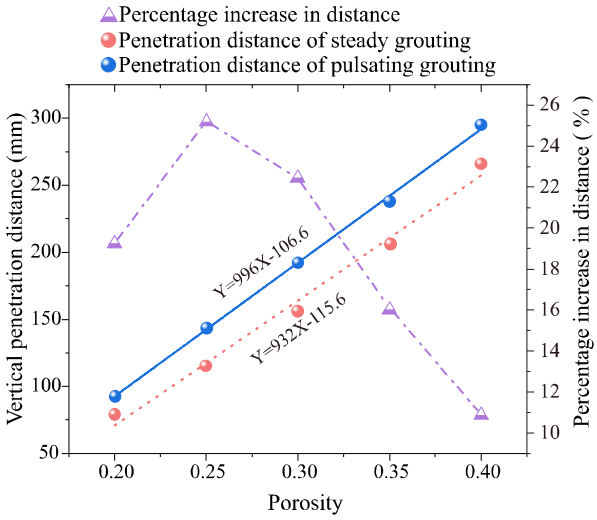


Figure 10. Effect of porosity on vertical penetration distance.

Figures 11 and 12 display the influence of the particle size of soil on penetration behavior. The penetration patterns of the lateral and vertical directions are similar to the influence of porosity. The expressions for lateral penetration distance and particle size for pulsating grouting and steady pressure grouting are as follows: Y = 306.3X + 11.6 and Y = 295.8X − 32.8, respectively. The expressions for vertical penetration distance and particle size of the two grouting methods are as follows: Y = 216.28X − 34.5 and Y = 190.45X − 38.7, respectively. As the particle size increases, the percentage increase in lateral distance gradually decreases. And that of vertical distance also initially rises and then decreases. This is also due to the smaller particle size, which results in more fluid flowing into the annular region during the pulsating grouting process.

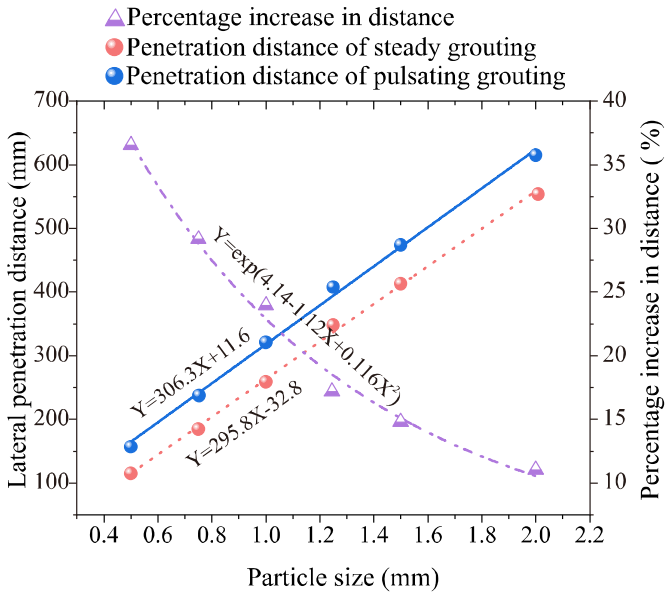


Figure 11. Effect of particle size on lateral penetration distance.

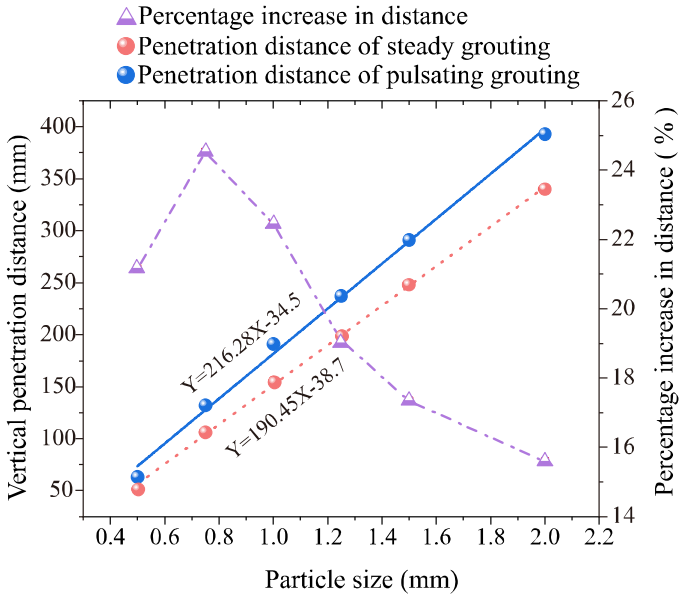


Figure 12. Effect of particle size on vertical penetration distance.

Figures 13 and 14 present the effect of viscosity on penetration behavior. As viscosity increases, the lateral penetration distance of pulsating grouting decreases from 549 mm to 294 mm, with the expression $Y = \exp(6.78 - 9.09X + 18.696X^2)$. Similarly, the penetration distance for steady pressure grouting decreases from 430 mm to 242 mm, with the expression $Y = \exp(6.52 - 8.92X + 19.18X^2)$. With the increase in viscosity, the percentage increase in distance gradually increases, which also demonstrates that pulsating grouting can achieve better performance in high-resistance conditions. As shown in Figure 14, the vertical penetration distance of pulsating grouting and steady grouting exhibits an exponential decrease. However, the percentage increase in distance follows a pattern of initially increasing and then decreasing. This is also due to the low resistance in the annular space. When the slurry viscosity is high, more slurry flows into the annular space under the influence of pulsating pressure.

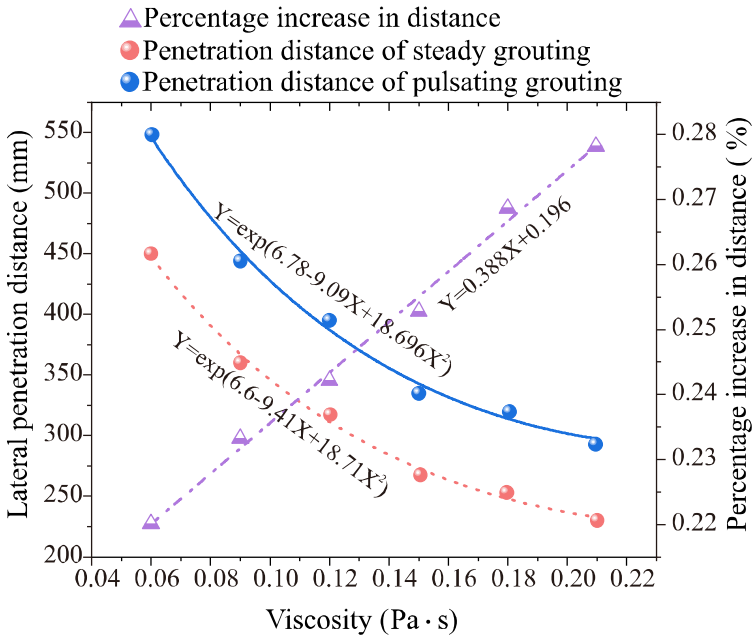


Figure 13. Effect of viscosity on lateral penetration distance.

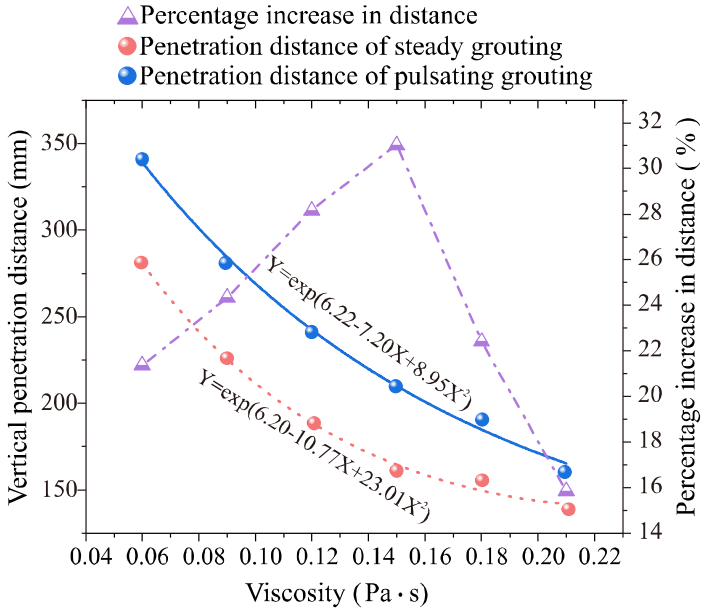


Figure 14. Effect of viscosity on vertical penetration distance.

As shown in Figures 15 and 16, the impact of back pressure on penetration distance is similar to viscosity. This is because the increases in back pressure and viscosity both increase flow resistance. With the increase in back pressure, both the lateral and vertical penetration distances of the tow grouting methods exhibit an exponential decrease. The percentage increase in the lateral distance gradually increases with the increase in back pressure, while the percentage increase in the vertical distance first increases and then decreases.

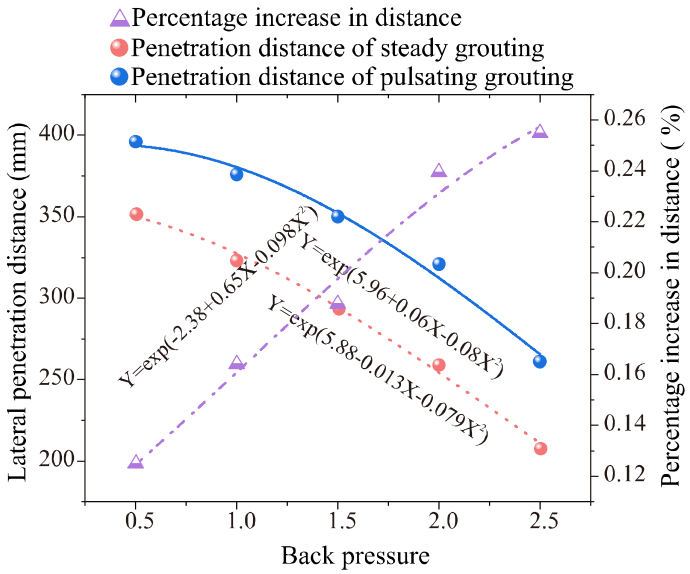


Figure 15. Effect of back pressure on lateral penetration distance.

Figures 17 and 18 present the impact of grouting pipe length on penetration distance. With the increase in the length of the grouting pipe, the lateral penetration distance for both grouting methods decreases exponentially. As the grouting depth increased from 2 m to 8 m, the lateral dispersion distance for steady pressure grouting decreased from 259 mm to 238 mm. The lateral dispersion distance for pulsatile grouting decreased from 321 mm to 291 mm. The increase in proportion falls within the range of 23.9% to 22.2%. The results also show that vertical penetration distance remains relatively unchanged. This is because, although the length of the grouting pipe has increased, the pressure in the grouting pipe

remains unchanged, which has a relatively small impact on vertical penetration. However, as the slurry spreads upward along the annular space, there is a gradual loss of pressure, which weakens the pulsation effect.

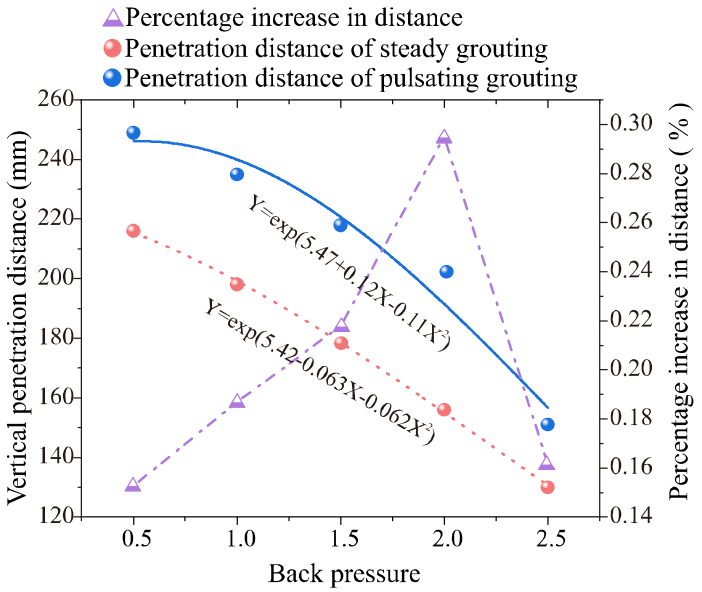


Figure 16. Effect of back pressure on vertical penetration distance.

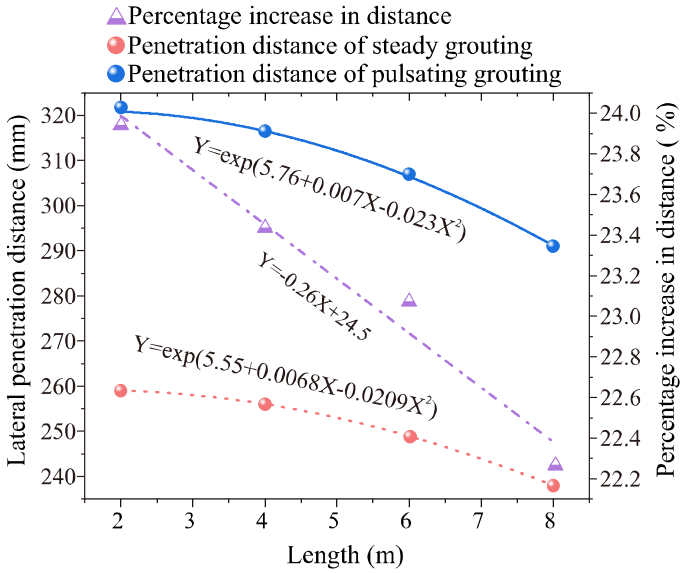


Figure 17. Effect of length of grouting pipe on lateral penetration distance.

It can be observed that there is a connection between different parameters and the dispersion behavior of the slurry. Regarding the lateral distance, the greater the flow resistance, the better the performance of pulsating grouting. However, for vertical dispersion distance, there is a critical value, and when the flow resistance is too high, the performance of the pulsating slurry decreases.

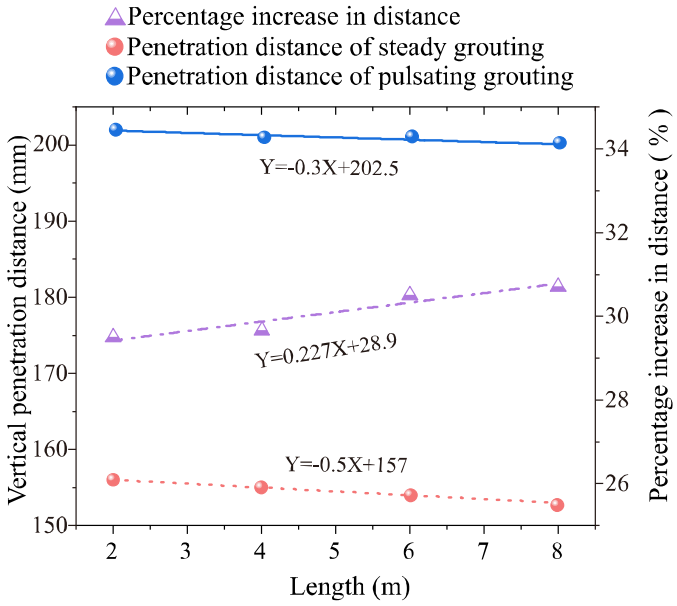


Figure 18. Effect of length of grouting pipe on vertical penetration distance.

4. Conclusions

This study compared the penetration performance between high-frequency pulsation grouting and steady grouting. The slurry penetration shape was investigated and the flow fields of the two grouting methods were analyzed. The effects of pulsation parameters, soil properties, slurry viscosity, grout pipe length, and back pressure on the slurry penetration distance were conducted.

(1) The results show that the penetration distance of pulsation grouting is significantly greater than stable pressure grouting. The reason is the periodic changes of the flow field induced with pressure pulsations. It was also found that higher frequency results in a longer slurry penetration distance. However, as the pulsation amplitude increases, the slurry penetration distance first increases and then decreases. This is because part of the pulsation pressure values become smaller than the back pressure.

(2) As the porosity and particle size decrease, and the viscosity and back pressure increase, the percentage increase in lateral penetration distance becomes larger. This is because the pulsation effect can achieve favorable results under conditions of high flow resistance. The percentage increase in vertical penetration distance initially increases and then decreases. The reason is that when the flow resistance is too high, the slurry penetrates faster under the pulsating pressure, leading more slurry to flow into the annular channel with lower flow resistance. As the grouting pipe length increases, the vertical diffusion performance remains almost unchanged, while the percentage increase in lateral penetration distance decreases, which is caused by the weakening of the pressure pulsation effect.

(3) Compared to steady pressure grouting, pulsating grouting can reduce cost and construction time, and enhance engineering quality. In underground engineering projects like tunnels, underground chambers, and shafts, pulsating grouting can be employed to strengthen underground structures, improving their stability and reducing the risk of structural wear and damage. In the future, there is a need for the development of grout materials suitable for pulsatile grouting. Additionally, it may be worthwhile to consider the application of a multi-objective optimization approach to select pulsation parameters that are most suitable for specific operating conditions.

Author Contributions: Conceptualization, L.T.; Methodology, Y.L. and X.C.; Software, F.L.; Validation, J.L.; Investigation, X.Z. All authors have read and agreed to the published version of the manuscript.

Funding: This research was funded by the National Key Research and Development Program of China under grant number 2020YFC1807200 and the National Natural Science Foundation of China (grant number: 51978674).

Institutional Review Board Statement: Not applicable.

Informed Consent Statement: Not applicable.

Data Availability Statement: Not applicable.

Conflicts of Interest: The authors declare no conflict of interest.

References

1. Du, J.; Zhou, A.; Shen, S.-L.; Bu, Y. Fractal-based model for maximum penetration distance of grout slurry flowing through soils with different dry densities. *Comput. Geotech.* **2022**, *141*, 104526. [CrossRef]
2. Liu, Q.; Xu, X.; Tang, X. A numerical study of the influence of cyclic grouting and consolidation using TOUGH2. *Bull. Eng. Geol. Environ.* **2021**, *80*, 145–155. [CrossRef]
3. Du, J.; Bu, Y.; Shen, Z.; Cao, X. Maximum penetration depth and penetration time predicting model of cementing fluid flow through wellbore into weakly consolidated formation. *Fractals* **2019**, *27*, 1950132. [CrossRef]
4. Zhang, G.; Xiao, T.; Zhang, C. An indoor experimental study of loose soil strata pulsating and regulated filling, Hydrogeology and engineering geology. *Hydrogeol. Eng. Geol.* **2016**, *43*, 87–93. [CrossRef]
5. Dou, J.; Zhang, G.; Zhang, X. Dynamic response analysis of slurry-soil coupling in sandy soil based on pulsating grouting. *Rock Soil Mech.* **2021**, *42*, 3315–3327. [CrossRef]
6. Zhao, F. A review of pulsation grouting reinforcement techniques for water-rich fractured rock masses. *Technol. Wind* **2021**, 77–79. [CrossRef]
7. Ghafar, A.; Mentesidis, A.; Draganovic, A. An Experimental Approach to the Development of Dynamic Pressure to Improve Grout Spread. *Rock Mech. Rock Eng.* **2016**, *49*, 3709–3721. [CrossRef]
8. Zhang, C. *Experimental Study on the Formation of Soft Filling Simulation*; Changsha University of Science & Technology: Changsha, China, 2019.
9. Han, C.; Wei, J.; Zhang, W.; Zhou, W.; Yin, H.; Xie, D.; Yang, F.; Li, X.; Man, X. Numerical Investigation of Grout Diffusion Accounting for the Dynamic Pressure Boundary Condition and Spatiotemporal Variation in Slurry Viscosity. *Int. J. Geomech.* **2021**, *21*, 04021018. [CrossRef]
10. Wakita, S.; Aoki, K.; Mito, Y. Development of dynamic grouting technique for the improvement of low-permeable rock masses. In Proceedings of the 1st Kyoto International Symposium on Underground Environment, Kyoto, Japan, 17–18 March 2003; pp. 341–348. [CrossRef]
11. Mohammed, M.; Pusch, R.; Knutsson, S. Study of cement-grout penetration into fractures under static and oscillatory conditions. *Tunn. Undergr. Space Technol.* **2015**, *45*, 10–19. [CrossRef]
12. Wang, G.; Hong, B.; Wu, J.; Liu, X. Experimental Study on the Shear Properties of Soil around Piles with Permeation Grouting. *Appl. Sci.* **2022**, *13*, 621. [CrossRef]
13. Jaf, D.K.I.; Abdulrahman, P.I.; Mohammed, A.S.; Kurda, R.; Qaidi, S.M.; Asteris, P.G. Machine learning techniques and multi-scale models to evaluate the impact of silicon dioxide (SiO_2) and calcium oxide (CaO) in fly ash on the compressive strength of green concrete. *Constr. Build. Mater.* **2023**, *400*, 132604.
14. Sagar, R.V. Acoustic emission characteristics of reinforced concrete beams with varying percentage of tension steel reinforcement under flexural loading. *Case Stud. Constr. Mater.* **2017**, *6*, 162–176.
15. Li, S.; Pan, D.; Xu, Z.; Lin, P.; Zhang, Y. Numerical simulation of dynamic water grouting using quick-setting slurry in rock fracture: The Sequential Diffusion and Solidification (SDS) method. *Comput. Geotech.* **2020**, *122*, 103497. [CrossRef]
16. Wang, Y.-H.; Yang, P.; Li, Z.-T.; Wu, S.-J.; Zhao, Z.-X. Experimental-numerical investigation on grout diffusion and washout in rough rock fractures under flowing water. *Comput. Geotech.* **2020**, *126*, 103717. [CrossRef]
17. Wang, Z.; Guo, W.; Ding, W.; Liu, K.; Qin, W.; Wang, C.; Wang, Z. Numerical study on the hydrodynamic properties of bentonite slurries with Herschel-Bulkley-Papanastasiou rheology model. *Powder Technol.* **2023**, *419*, 118375. [CrossRef]
18. Wang, Y. *Numerical Simulation and Application of Polymer Grouting*; Southeast University: Nanjing, China, 2018.

Disclaimer/Publisher's Note: The statements, opinions and data contained in all publications are solely those of the individual author(s) and contributor(s) and not of MDPI and/or the editor(s). MDPI and/or the editor(s) disclaim responsibility for any injury to people or property resulting from any ideas, methods, instructions or products referred to in the content.